SWIR-Based Atmospheric Correction for Satellite Ocean Color Using Principal Component Analysis Decomposition over the La Plata River Highly Turbid Waters

Juan I. Gossn [#1], Robert Frouin[*2], Ana I. Dogliotti[#3], Francisco M. Grings[#4]

[#] *Quantitative Remote Sensing Group, Marine Division, Instituto de Astronomía y Física del Espacio, CONICET-UBA*
Int. Güiraldes 2620 (Pabellón IAFE, Ciudad Universitaria), C1428ZAA, Buenos Aires, Argentina

[1] gossn@iafe.uba.ar

[3] dogliotti@iafe.uba.ar

[4] verderis@iafe.uba.ar

[*] *Scripps Institution of Oceanography, University of California San Diego*
8622 Kennel Way, La Jolla, CA 92037, USA

[2] rfrouin@ucsd.edu

***Abstract*— The quality of information provided by ocean color imagery relies on the availability of an accurate atmospheric correction algorithm, which turns to be more complicated in highly turbid coastal regions, such as in the Río de la Plata River (RdP) (Argentina-Uruguay). In these waters, the usual black pixel assumption in the Near Infra-Red (NIR, 700-1000 nm) bands is often invalid due to high backscattering from suspended particulate matter (SPM) present in the water. In this work, an atmospheric correction scheme is presented to estimate water reflectance in the 865 nm NIR band. This scheme is based on shifting the black pixel assumption to the Short-Wave-Infra-Red (SWIR, 1000-3000 nm) bands and a Principal Component Analysis (PCA) decomposition of simulated atmosphere-interface reflectances. To estimate the latter component in the top of atmosphere (TOA) signal, the weight of each of these PCA eigenvectors is determined from the SWIR bands in a per-pixel-basis. The algorithm was theoretically tested from a set of simulated TOA reflectances performed considering atmospheric conditions and in-situ water reflectance data from RdP. Four schemes were analyzed using different sets of SWIR bands present in MODIS and SABIA-Mar (future Argentinian-Brazilian ocean color mission) sensors. These sets differ from each other in their correlation to the NIR and the validity of the black pixel assumption. Without considering instrument noise, the scheme with better performance is the one in which water reflectance is negligible in the SWIR bands considered: 1640 nm (SABIA-Mar/MODIS) and 2130 nm (MODIS).**

***Resumen*— La calidad de información provista por imágenes de color del mar está sujeta a la disponibilidad de un algoritmo de corrección atmosférica preciso, condición más complicada en casos de aguas costeras altamente turbias, como las del Río de la Plata (RdP) (Argentina-Uruguay). En estos escenarios, la habitual asunción de píxel negro en las bandas del infrarrojo cercano (NIR, por sus siglas en inglés, 700-1000 nm) se torna usualmente inválida, debido a la alta retrodispersión causada por el material particulado en suspensión (MPS) presente en el agua. En este trabajo, se presenta un esquema de corrección atmosférica para estimar la reflectancia marina en la banda del NIR centrada en 865 nm. Este esquema se basa en desplazar la asunción de píxel negro a las bandas del infrarrojo de onda corta (SWIR, por sus siglas en inglés, 1000-3000 nm) y en la descomposición por Análisis de Componentes Principales (PCA) de las reflectancias simuladas de atmósfera-interfase. Para estimar estas componentes en la señal de tope de atmósfera (TOA), el peso de cada uno de estos autovectores por PCA es determinado a partir de las bandas en el SWIR para cada píxel. El algoritmo fue testeado teóricamente a partir de un conjunto de simulaciones a TOA en que fueron introducidas condiciones atmosféricas y mediciones in-situ de reflectancias marinas del RdP. Cuatro esquemas fueron analizados combinando distintos conjuntos de bandas SWIR presentes en los sensores MODIS y SABIA-Mar (futura misión satelital de color del mar argentino-brasileña). Estos conjuntos se diferencian entre sí por su correlación con el NIR y la validez del píxel negro. Sin considerar el ruido del sensor, el esquema con mejor desempeño corresponde a aquel donde la señal marina es despreciable para las bandas SWIR consideradas: 1640 nm (SABIA-Mar/MODIS) y 2130 nm (MODIS).**

I. Introduction

The NASA standard atmospheric correction algorithm applied to Sea-WIFS (Sea Wide Field-of-View Sensor) and MODIS (Moderate Resolution Imaging Spectroradiometer) imagery uses two bands in the Near Infra-Red (NIR) at 765 and 865 nm, assuming zero water-leaving radiance contribution (black pixel) at these bands [1]. The process consists in i) estimating the atmospheric component from these bands (taking advantage of the absence of the marine signal), and ii) extrapolating the signal to the visible (VIS) bands (the ones carrying useful information). For the cases in which there exists some mild marine signal in the NIR, an iterative process is run to estimate this component; subtract it from the total signal to recover the black pixel condition, and proceed as usual for the extrapolation to the VIS [2]. In waters with elevated concentrations of suspended particulate matter (SPM), which backscatters strongly in the NIR, the signal at 765 and 865 nm is not moderate anymore and even exceeds sometimes the saturation values of the sensor. In these cases, this iterative procedure is no longer operative and other alternatives are needed.

Many authors have proposed the Short-Wave-Infra-Red (SWIR) bands to be used as an alternative (e.g. 1240, 1640

and 2130 nm in MODIS) [3]-[5]. At this spectral region, water absorption drastically increases making the black pixel assumption still hold, thus making these bands very helpful to perform atmospheric correction in highly turbid waters scenarios. It has been found that in the region of maximum turbidity in the RdP, reflectance at 1240 nm MODIS band is still not negligible [6], thus undermining the performance of the standard NIR-SWIR algorithm developed by Shi-Wang 2007 [3] and Wang-Shi 2007 [4] in this region. As an alternative it has been proposed to use auxiliary clear-water regions in the images where the black pixel assumption holds and use the aerosol information retrieved from these pixels in the whole image [7].

In the present work, a preliminary atmospheric correction scheme is presented and theoretically tested to estimate the marine reflectance in the NIR band at 865 nm so it can be subtracted from the total signal to recover the black pixel condition. It essentially consists of decomposing the atmospheric signal into Principal Components (PCA), and estimate their corresponding weights using the reflectance in the SWIR bands at each pixel. The SWIR bands that were tested correspond to MODIS and the future Argentinean-Brazilian Ocean-Color Satellite Mission SABIA-Mar sensors. An advantage of this procedure is that it relies neither on auxiliary clear water regions in the images (such as in Dogliotti *et al.* 2011 [7]) nor on decision trees to define turbid and non-turbid waters (such as in the NIR-SWIR approach [4]) that yield difficulties in the transition zones.

II. Simulations and Field Data

In order to simulate the top-of-atmosphere (TOA) reflectances for the SABIA-Mar and MODIS sensors, the CNES-SOS v5.0 (SOS: Successive Orders of Scattering) radiative transfer code [8] was run using a set of input values specified by field data collected in the RdP region and by standard values found in the literature.

The spectral range covered encompasses all MODIS and SABIA-Mar bands in the VIS-NIR-SWIR region (Table I). In this table, the bands where the marine reflectance is not negligible in turbid waters and needs to be estimated is indicated in orange and the SWIR bands (assumed to be black) used for the atmospheric correction are shown in red. The reflectances for each band were computed using the corresponding Spectral Response Functions (SRF) reported by NASA [9] in the case of MODIS, and using square shaped SRFs defined by the band centers and widths in the case of SABIA-Mar sensor.

TABLE I

Ocean Color Bands in SABIA-Mar and Modis

SABIA-Mar			MODIS		
Band	**Center [nm]**	**Width [nm]**	**Band**	**Center [nm]**	**Width [nm]**
B00	380	15.0			
B01	412	10.0	**B08**	412	15
B02	443	10.0	**B09**	443	10
B03	490	10.0	**B03**	469	20
B04	510	10.0	**B10**	488	10
B04B	531	10.0	**B11**	531	10
B05	555	10.0	**B12**	551	10
B06	620	10.0	**B04**	555	20
B07	665	10.0	**B01**	645	50
B08	680	7.5	**B13**	667	10
B09	710	10.0	**B14**	678	10
B10	750	10.0	**B15**	748	10
B11	765	10.0	**B02**	859	35
B12	865	20.0	**B16**	869	15
B13	1044	20.0	**B05**	1240	20
B14	1240	20.0	**B06**	1640	35

To account for the Rayleigh scattering effect produced by air molecules, Rayleigh optical thickness and molecular depolarization factor values were obtained from Bodhaine *et al.* 1999 [10]. The aerosol atmospheric scenarios used correspond to expectable combinations of the standard World Meteorological Organization (WMO) scenarios [11] (Continental, Maritime, Urban) for the region (see Table II).

TABLE II

Expectable Aerosol Scenarios (Based on WMO)

Scenario ID	WMO scenario [%]		
	Urban	**Continental**	**Maritime**
1	**100**	**0**	**0**
2	**0**	**100**	**0**
3	**50**	**50**	**0**
4	**0**	**80**	**20**
5	**20**	**80**	**0**
6	**80**	**20**	**0**

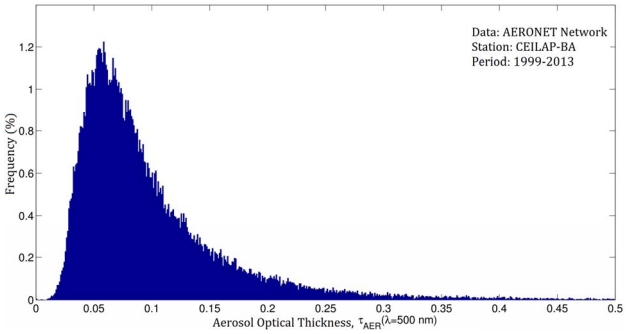

Fig. 1. Histogram of aerosol optical depth at 500 nm, as measured in CEILAP-BA (AERONET), period 1999-2013.

The aerosol optical depths at 500 nm, $\tau_{AER}(500)$, were determined from the photometric measurements done at CEILAP-BA station [12], corresponding to the AERONET network [13], in the period 1999-2013 (Fig. 1). These values are log-normally distributed in the range 0.00-0.50 with a mode value of 0.06.

The marine reflectance values used (named RdP 1, 2, 3 and 4, see Fig. 2) correspond to measurements collected during two field campaigns in Punta Piedras, located in the maximum turbidity zone of the RdP, performed on February 27 and April 30, 2013 (stations PP01-07/02 and PP02-09/11 respectively). Water reflectance (350-2500 nm) was measured using an ASD Fieldspec FR spectrometer. The

turbidity values measured during these campaigns increased from RdP1 to RdP4, with values ranging from 16 FNU (Formazin Nephelometric Units) in RdP1 to >1000 FNU (sensor saturation) in RdP4 and were obtained using a portable HACH 2100P ISO turbidimeter (see *Dogliotti et al. 2011* for locations and details [14]). Over these reflectances, the effect of whitecaps was added in the simulations, which was considered as dependent on wind speed, as described in [15]-[17].

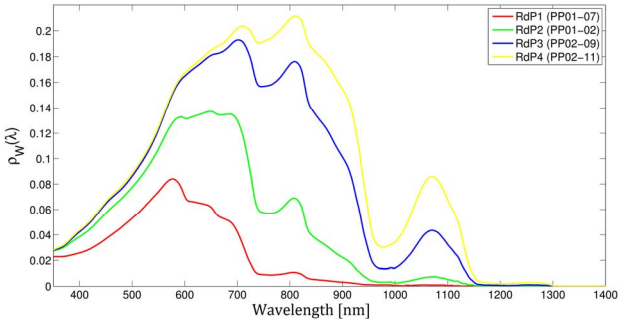

Fig. 2. Water reflectances (used as input to SOS code) obtained from field campaigns in Punta Piedras (Southern RdP) in the turbidity front region on February 27 and April 30, 2013.

The range of surface wind speeds (used by SOS to compute the specular surface term and the fraction of the surface covered by whitecaps) was selected based on the measured wind values in the Aeroparque Meteorological Station for the period 1976-2014 (Fig. 3). The most probable wind speeds measured correspond to the range 4-6 m/s, and winds above 14 m/s were registered in much less than 1% of the measurements.

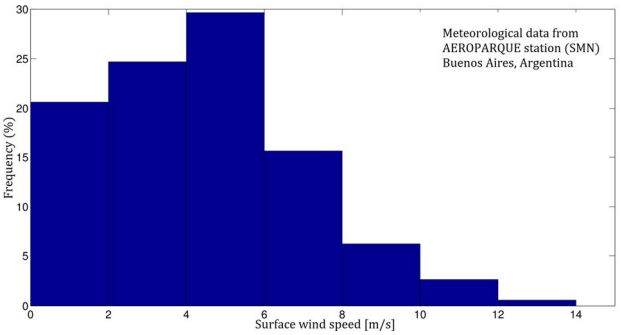

Fig. 3. Wind speed distribution of measurements taken at Aeroparque Meteorological Station, Buenos Aires, Argentina. Period 1976-2014.

The I, Q and U components of the Stokes parameters were computed (i.e. polarization effects were taken into account, see Lenoble *et al.* 2007 for more details [8]) for a maximum of 20 scattering events for each photon. The rest of the inputs required by the SOS were fixed from standard values found in the literature. All the values used are summarized in Table III.

TABLE III

INPUT PARAMETERS FOR THE CNES-SOS CODE

CNES-SOS Input Parameter	Inserted Values
λ (Wavelength)	300:2:2200 nm
θ_S (Solar zenith angle)	0°:5°:60°
θ_V (Viewing zenith angle)	0°:5°:70°
Δφ (Relative azimuth angle)	0°:5°:180°
$\tau_{RAY}(\lambda)$ (Rayleigh Opt. Thickness)	Bodhaine et al. (1999)
$\delta_{RAY}(\lambda)$ (Molecular depolarization factor)	
H_{RAY} (Molecular height e-folding)	8 km
dV/dlnr (Aerosol granulometry)	Scenarios 1-6 (see text)
τ_{AER} (Aerosol Opt. Thickness at 500 nm)	
H_{AER} (Aerosol height e-folding)	2 km
n_{H2O} (relative air-water refractive index)	1.334
$\rho_W(\lambda)$ (Marine reflectance)	RdP 1-4 (see text)
w (Wind speed)	0:5:10 m/s
n_{max} (Maximum order of scattering)	20
I_{pol} (Polarization flag)	1 (Polarization ON)

Two separate sets of simulations were run. A first one was generated introducing a black ocean in order to obtain the signal corresponding to the atmosphere and the atmosphere-water interface reflection, defined as ρ_{ATM}. From this set, the PCA decomposition was computed, which yielded an orthogonal base of principal components, that correspond to the eigenvectors of the variance-covariance matrix of the set, being the j-th component expressed as

$$e_j^{PCA}(\lambda = 865, SWIR), \quad (1)$$

where j=1,...,N+1, being N+1 equal to the number N of SWIR bands used for the correction (N=2 or 3, depending on the scheme) plus the NIR band at 865 nm.

The second set corresponds to the simulated signal at TOA with non-black ocean, i.e. including the water reflectances shown in Fig. 2. This set of data was used to test theoretically the performance of the atmospheric correction.

III. ALGORITHM DESCRIPTION

The following list describes the PCA algorithm

- After i) assuming the black pixel condition in the SWIR bands; ii) discarding regions of elevated sun glint values (ρ_{SG}>0.050); iii) neglecting the whitecaps effect and the gaseous absorption (quite absent in the bands considered), the following expression for the TOA reflectance is obtained:

$$\begin{aligned} \rho_{TOA}(865) &\approx t(865)\rho_W(865) + \rho_{ATM}(865) \\ \rho_{TOA}(SWIR) &\approx \rho_{ATM}(SWIR) \end{aligned}, \quad (2)$$

being t(λ) the diffuse atmospheric transmittance and $\rho_W(\lambda)$ the marine reflectance.

- Using the Principal Components of the ρ_{ATM} signal (first set of simulations, Eq. (1)) and the TOA reflectances in the SWIR bands, ρ_{TOA}(SWIR), the projections a_1 and a_2 of the first 2 principal components (hereafter N=2 for brevity) were computed inverting the following linear system:

$$\begin{pmatrix} \rho_{TOA}(SW1) \\ \rho_{TOA}(SW2) \end{pmatrix} = \begin{pmatrix} e_1^{PCA}(SW1) & e_2^{PCA}(SW1) \\ e_1^{PCA}(SW2) & e_2^{PCA}(SW2) \end{pmatrix} \begin{pmatrix} a_1 \\ a_2 \end{pmatrix}, \quad (3)$$

- Subsequently, $\rho_{ATM}(865)$ is obtained out of these projections:

$$\rho_{ATM}(865) \approx a_1 e_1^{PCA}(865) + a_2 e_2^{PCA}(865), \qquad (4)$$

and subtracted from the signal, leaving the component t(865)ρ_W (865) (see Eq. (2)).

- Finally, the remaining signal is divided by the diffuse transmittance at 865 nm, t(865), following the expression suggested in Tanre *et al.* 1979 [18]:

$$t(865) = \exp\{-[0.52\tau_{RAY}(865) + 0.16\tau_{AER}(865)]\mu\}, \qquad (5)$$

in which the coefficients 0.52 and 0.16 represent the back-to-total scattering fractions for molecules and aerosols, respectively; Rayleigh and aerosol optical thicknesses at 865 nm are expressed respectively as $\tau_{RAY}(865)$ and $\tau_{AER}(865)$, and μ accounts for the air mass factor, $\mu = \cos^{-1}(\theta_S) + \cos^{-1}(\theta_V)$, where θ_S and θ_V are the solar and viewing zenith angles. The value of $\tau_{AER}(865)$ was fixed at the mode value obtained from the CEILAP-BA AERONET station: $\tau_{AER}(865)$=0.04. The difference between this value and the actual one may lead to errors in the transmittance factor of 3-5% in the worst cases.

Four different schemes were proposed with different MODIS (MD) and SABIA-Mar (SM) SWIR band combinations (shown between parentheses). They are:

- PCA-2-SM (1240, 1640): uses 1240 nm band, which can have slightly non-zero marine signals in RdP (see Fig. 2).
- PCA-2-MD (1640, 2130): Both bands used are effectively free from marine signal.
- PCA-3-SM (1044, 1240, 1640): Uses 1044 nm band, with moderate/high marine signals in RdP (see Fig. 2).
- PCA-3-MD (1240, 1640, 2130): 1240 nm band was added to PCA-2-MD to enhance correlation with 865 nm.

A scheme summarizing the methodology is shown in Fig. 4.

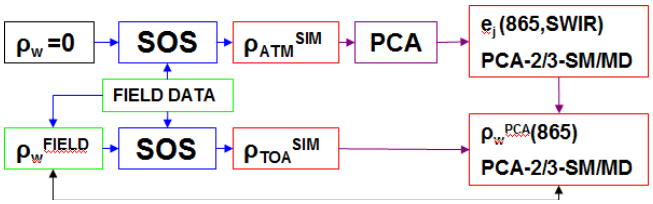

Fig. 4. Global scheme of the methodology developed in the present work. In green boxes, the inputs, in red, the outputs. Blue boxes/arrows correspond to the forward model, and magenta boxes/arrows to the inverse.

IV. Results and Discussion

Some examples of TOA refleclectances retrieved by SOS using input parameters (indicated in Table III) are shown in Fig. 5. In the figure, the atmospheric scenario was set to 80% Continental + 20% Urban (Table II) for $\tau_{AER}(500)$=0.5 (green lines), while atmospheres free of aerosols correspond to $\tau_{AER}(500)$=0 (red lines), and scenarios corresponding to field measured reflectance spectra RdP1 and 4 (blue lines) were considered. The TOA signal seems consistent with what is expected, i.e., the shape and high signal associated to Rayleigh scattering is clearly observed in the blue region and the strong marine signal in the 500-1000 nm region; as well as becoming close to zero in the scenarios free of aerosols in the SWIR, while in the scenarios with aerosols still persists a strong flat signal in this spectral region.

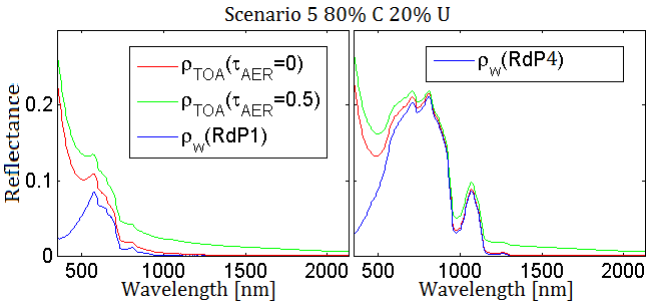

Fig. 5. Simulated reflectances at TOA, corresponding to no aerosols and atmospheric scenario 5 with $\tau_{AER}(500)$= 0.5 (red and green lines respectively) and field marine reflectances (blue lines), for RdP measurements 1 (left) and 4 (four).

This behavior of the TOA signal as well as in the rest of the marine and atmospheric scenarios (not plotted here for brevity) brings confidence in the plausibility of the SOS simulations. Regarding the set simulated with ρ_W=0 (i.e. ρ_{TOA}=ρ_{ATM}), the scatter plots between the signal at the different bands is shown in Fig. 6.

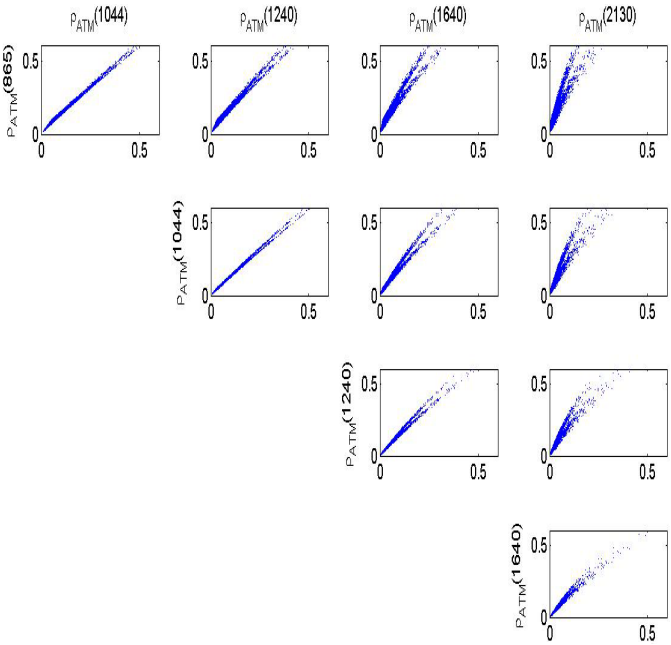

Fig. 6. Scatter plots of the whole set of ρ_{ATM} simulations for the NIR-SWIR bands considered (MODIS and SABIA-Mar band at 1044 nm)

These scatter plots show that there exists a high correlation between the ρ_{ATM} signals of the different SWIR bands; but this correlation tends to decrease as the spectral distance between the corresponding bands increases. The PCA scheme (Eqs. (3)-(5)) strongly relies on this high correlation, meaning that using the most distant bands (i.e., the less correlated to 865 nm) may bring more dispersion when discarding the Principal Components with less variance associated. So this means that there exists a trade-off situation between i) the validity of the black pixel assumption (entirely valid at 1640 and 2130 nm) and ii) the correlation between ρ_{ATM} at the corresponding SWIR band and at 865 nm (worse for 1640 and 2130 nm bands). The

particularly separated plumes observed in the subplots corresponding to the highest spectral distances among bands (e.g. 865 vs 2130 nm, top-right corner, Fig. 6) are related to the presence of oceanic aerosols in the atmospheric scenarios proposed (particularly, Scenario 4, see Table II), which contain different absorption properties than the rest of the aerosol modes [11].

The results of the PCA atmospheric schemes for the four combinations of the MODIS/SABIA-Mar SWIR bands, described in detail in Section III, are shown in Fig. 7. For each scheme a linear regression was performed, shown with solid blue lines (slope, intercept and Pearson coefficient reported on each inset), while the 1:1 relation is indicated with a dashed black line. The PCA-3-SM (1044, 1240, 1640) scheme (third subplot, blue dots) presents highly underestimated values, mainly because it relies on the 1044 nm band, which presents a considerably high marine signal (see Fig. 2). For instance, this scheme is the one that better performs in the water scenario RdP 1, corresponding to the lowest $\rho_w(859)$ (Field) (vertical blue strip of the data in this subplot, see also Fig. 9). The rest of the PCA-derived reflectances from the other schemes present much higher scatter. This is linked to the fact that these schemes use bands further apart in the spectrum compared to PCA-3-SM, i.e., less correlated to 865 nm. For instance, the PCA-2-MD (1640, 2130) scheme (second subplot, green dots), which uses the two bands located farthest to 865 nm band presents the highest scatter.

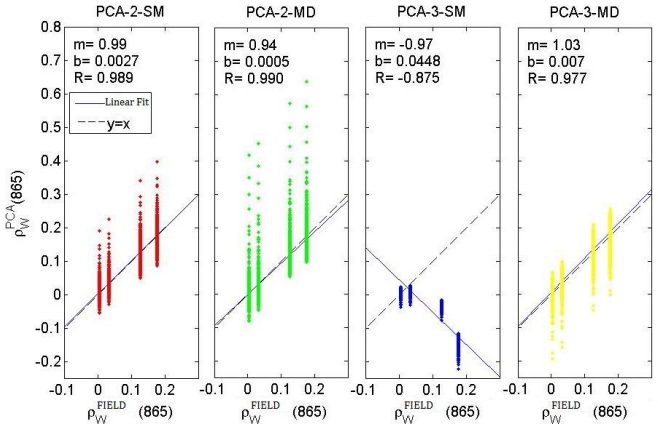

Fig. 7. Water reflectance $\rho_W(865)$ (FIELD) vs. $\rho_W(865)$ (PCA) for the four schemes proposed (PCA-2/3-SM/MD) and the four water scenarios considered, RdP 1-4 (four different values in x axis).

A series of subsets of the ρ_{TOA} simulations were defined by setting reduced ranges for the input values reported in Table III to see if there existed a particular subset of the whole parametric set that resulted in the worse performances for the schemes (i.e. the parameter values associated to the most distant dots to the y=x line in Fig. 7). In particular, constraining the ranges of $\tau_{AER}(500nm)$ (aerosol optical thickness at 500 nm) and θ_V (viewing zenith angle) by the additional conditions:

$$\begin{aligned} &\tau_{AER}(500nm) < 0.4\,, \\ &\theta_V < 60° \end{aligned} \qquad (6)$$

a new ρ_{TOA} set is obtained and the results of the PCA performances are shown in Fig. 8. The conditions expressed in Eq. (6) exclude scenarios where: i) $\tau_{AER}(500nm)$ exceeds 0.4, i.e. very rare conditions based on in-situ measured values as shows Fig. 1, and ii) where the sensor is 30° or less above the horizon, i.e. corresponding to pixels located generally at the edge of the images that are usually discarded given the decreasing in the water reflectance that reaches TOA due to the larger atmospheric path length. The performance of the PCA algorithm over this reduced set is substantially improved over all schemes, except for PCA-3-SM (1044, 1240, 1640), that still presents high underestimation associated to non-zero water reflectance in 1044 nm band.

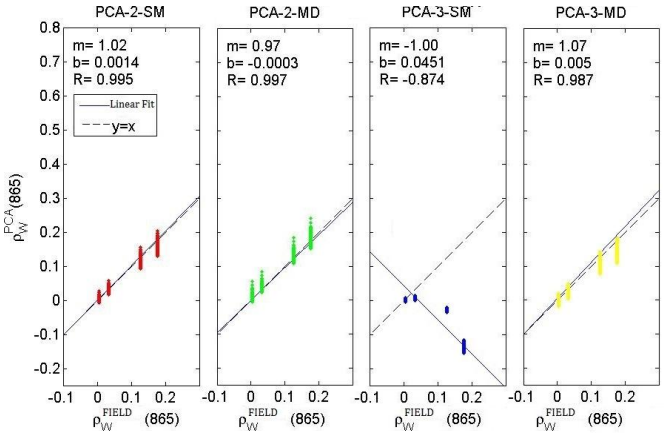

Fig. 8. Same as Fig. 7 but for the reduced set as described in Eq. (6).

Finally, the absolute mean errors are shown in Fig. 9, for each of the schemes (PCA-2/3-SM/MD) and water scenarios (RdP 1-4), corresponding to the reduced ρ_{TOA} set defined by Eq. (6). For the less turbid scenario (RdP1), with virtually no water signal in any of the tested SWIR bands, the schemes that show better performances are the ones that include the bands closet to 865 nm, i.e. the bands that exhibit highest correlation to 865 nm (in the ρ_{ATM} signal, see Fig. 6). As the water scenarios exhibit higher water signals in the 1044 and 1240 nm bands, the schemes that use these bands tend to perform progressively worse, especially PCA-3-SM (1044, 1240, 1630, blue line), that correspond to the only scheme that includes the 1044 nm band. In the most turbid scenario (RdP4), with higher signal in the NIR-SWIR region, the scheme that performs better is PCA-2-MD (1640, 2130, green line): this can be attributed to the fact that this scheme is the only one that uses bands where the water signal is negligible.

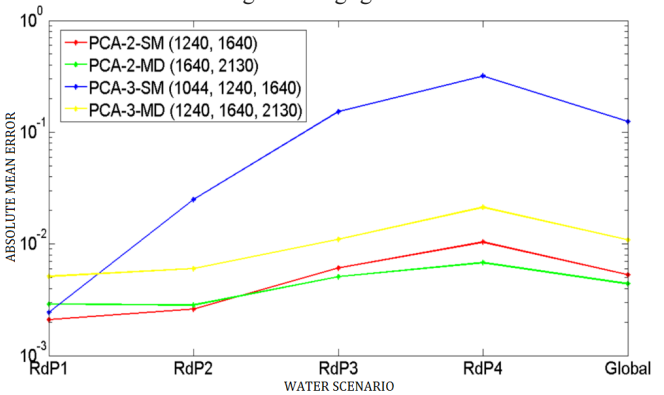

Fig. 9. Mean absolute error for the different PCA schemes and field measured water reflectance, as well as the global performance.

V. Conclusions

In the present paper, an atmospheric correction algorithm designed to estimate the marine signal at 865 nm band present in MODIS and SABIA-Mar sensors is described. This algorithm consists of decomposing a set of simulated atmospheric-interface reflectances into Principal Components, and estimating their corresponding weights using the top-of-atmosphere reflectance in the SWIR (1000-3000 nm) bands at each pixel. The algorithm was theoretically tested using a set of simulated top-of-atmosphere reflectance data. All simulations were obtained using the CNES-SOS radiative transfer code, which was run using input parameters constrained using measured atmospheric conditions and field data collected in Río de la Plata River (Argentina-Uruguay) and different standard aerosol scenarios. The RdP is one the most turbid rivers in the world and due to its high particulate matter concentrations, these waters infringe the zero-marine signal assumption made by standard atmospheric correction algorithms in the NIR and even at the SWIR 1044 nm and 1240 nm bands.

Four different schemes were proposed which used different combinations of SWIR bands present in MODIS and SABIA-Mar sensors. Two conditions influenced the performance of each of the schemes: the presence of marine signal in the correcting (SWIR) bands and the spectral distance to the band of interest, i.e. 865 nm. Schemes using the nearest bands (1044, 1240 nm) had better performances for clear water scenarios while the ones that used black-ocean bands where the ocean is actually black (1640, 2130 nm) were the ones that performed better for the extremely turbid scenarios.

Acknowledgment

This research was supported by the ANPCyT (National Agency for Scientific and Technological Research of Argentina) PICT 2010-1831, PICT 2014-0455, and the CONICET (National Council for Scientific and Technological Research of Argentina) PIP 112 20120100350 Projects. The technical support of Pablo Perna, from Instituto de Astronomía y Física del Espacio, is gratefully acknowledged. The authors also thank the CONAE (Argentina's Space Activity National Comission) for providing the ASD Spectroradiometer used for the measuremets; Gerardo Lascala from the SMN (Argentina's National Meteorological Service) for providing meteorological data series for Aeroparque; Lidia Otero from CEILAP-BA (AERONET station in Buenos Aires, Argentina), and Bruno Lafrance from LOA (Laboratorie d'Optique Atmospherique, France), who provided us useful remarks on the SOS code.

References

[1] Gordon, H. R., y Wang, M. (1994), "Retrieval of Water-Leaving Radiance and Aerosol Optical Thickness over the Oceans with SeaWiFS: A Preliminary Algorithm", *Applied Optics*, 33, 443-452.

[2] R. P. Stumpf, R. A. Arnone, J. R. W. Gould, P. M. Martinolich, and V. Ransibrahmanakul, "A Partially Coupled Ocean-Atmosphere Model for Retrieval of Water-Leaving Radiance from SeaWiFS in Coastal Waters," *in Patt, F.S., et al., 2003: Algorithm Updates for the Fourth SeaWiFS Data Reprocessing. NASA Tech. Memo. 206892, National Aeronautics and Space Administration, Goddard Space Flight Center*, Greenbelt, MD (2003).

[3] Shi, W., Wang, M., "Detection of Turbid Waters and Absorbing Aerosols for the MODIS Ocean Color Data Processing," *Remote Sensing of Environment*, vol. 110, pp. 149–161, Sep. 2007.

[4] Wang, M., Shi, W., (2007), "The NIR-SWIR Combined Atmospheric Correction Approach for MODIS Ocean Color Data Processing," *Opt. Express* 15, 15722-15733.

[5] Chen, J., Yin, S., Xiao, R., Xu Q., Line C., "Deriving Remote Sensing Reflectance from Turbid Case II Waters Using Green-Shortwave Bands Based Model," *Advances in Space Research* 53 (2014) 1229-1238.

[6] Shi, W., Wang, M., "An Assessment of the Black Ocean Pixel Assumption for MODIS SWIR Bands," *Remote Sensing of Environment*, 113 (2009), 1587-1597.

[7] Dogliotti, A.I., Ruddick, K., Nechad, B., and Lasta, C. (2011), "Improving Water Reflectance Retrieval from MODIS Imagery in the Highly Turbid Waters of La Plata River," *Proceedings of VI International Conference: Current problems in optics of natural waters (ONW 2011). Publishing House Nauka of RAS,* 2011. p. 152. Saint-Petersburg, Russia. 6-10 September, 2011.

[8] J. Lenoble, M. Herman, J.L. Deuzé, B. Lafrance, R. Santer, D. Tanré, "A Successive Order of Scattering Code for Solving the Vector Equation of Transfer in the Earth's Atmosphere with Aerosols," *Journal of Quantitative Spectroscopy & Radiative Transfer* 107 (2007) 479-507.

[9] MODIS Spectral Response Functions, available at http://oceancolor.gsfc.nasa.gov/DOCS/RSR_tables.html

[10] Bodhaine, B. A.,Wood, N. B., Dutton, E. G., Slusser, J. R., "On Rayleigh Optical Depth Calculations," *Journal of atmospheric and oceanic technology,* vol. 16, 21 January 1999 and 3 May 1999.

[11] World Climate Research Programme, "A Preliminary Cloudless Standard Atmosphere for Radiation Computation," *WCP 112, WMO/TD Report No 24,* Geneva, Switzerland , March 1986

[12] CEILAP Website: divisionlidar.com.ar/

[13] AERONET Website: aeronet.gsfc.nasa.gov/

[14] Dogliotti, A. I., Lutz, V.A., Segura, V., "Estimation of Primary Production in the Southern Argentine Continental Shelf and Shelf-Break Regions Using Field and Remote Sensing Data", *Remote Sensing of Environment*, vol 140, pp. pp. 497–508, Jan. 2014, doi:10.1016/j.rse.2013.09.021

[15] Koepke, P., "Effective Reflectance of Oceanic Whitecaps," *Applied Optics,* Vol. 23, Issue 11, pp. 1816-1824 (1984), http://dx.doi.org/10.1364/AO.23.001816

[16] Frouin, R., M. Schwindling, P.-Y. Deschamps (1996). "Spectral Reflectance of Sea Foam in the Visible and Near Infrared: In-situ Measurements and Remote Sensing Applications," *J. Geophys. Res.* 101, 14361-14371.

[17] Nicolas, J.-M., P.-Y. Deschamps, and R. Frouin (2001). "Spectral Reflectance of Oceanic Whitecaps in the Visible and Near Infrared: Aircraft Measurements over Open Ocean," *Geophys, Res. Lett.*, vol. 28, 4445-4448.

[18] D. Tanre, Herman, P. Y. Deschamps, and A. de Leffe, "Atmospheric Modeling for Space Measurements of Ground Reflectances, Including Bidirectional Properties," *Applied Optics,* Vol. 18, Issue 21, pp. 3587-3594 (1979) •doi: 10.1364/AO.18.003587